frontiers in Earth Science

ORIGINAL RESEARCH
published: 21 December 2020
doi: 10.3389/feart.2020.559624

Aftershock Rate Changes at Different Ocean Tide Heights

*P. N. Shebalin and A. A. Baranov**

Institute of Earthquake Prediction Theory and Mathematical Geophysics, Russian Academy of Sciences, Moscow, Russia

The differential probability gain approach is used to estimate quantitatively the change in aftershock rate at various levels of ocean tides relative to the average rate model. An aftershock sequences are analyzed from two regions with high ocean tides, Kamchatka and New Zealand. The Omori-Utsu law is used to model the decay over time, hypothesizing an invariable spatial distribution. Ocean tide heights are considered rather than phases. A total of 16 sequences of M ≥6 aftershocks off Kamchatka and 15 sequences of M ≥6 aftershocks off New Zealand are examined. The heights of the ocean tides at various locations were modeled using FES 2004. Vertical stress changes due to ocean tides are here about 10–20 kPa, that is, at least several times greater than the effect due to Earth tides. An increase in aftershock rate is observed by more than two times at high water after main M ≥6 shocks in Kamchatka, with slightly less pronounced effect for the earthquakes of M = 7.8, December 15, 1971 and M = 7.8, December 5, 1997. For those two earthquakes, the maximum of the differential probability gain function is also observed at low water. For New Zealand, we also observed an increase in aftershock rate at high water after thrust type main shocks with M ≥6. After normal-faulting main shocks there was the tendency of the rate increasing at low water. For the aftershocks of the strike-slip main shocks we observed a less evident impact of the ocean tides on their rate. This suggests two main mechanisms of the impact of ocean tides on seismicity rate, an increase in pore pressure at high water, or a decrease in normal stress at low water, both resulting in a decrease of the effective friction in the fault zone.

Keywords: ocean tides, Kamchatka, New Zealand, FES 2004, Omori-Utsu law, differential probability gain, pore pressure, effective friction

OPEN ACCESS

Edited by:
Antonella Peresan, Istituto Nazionale di Oceanografia e di Geofisica Sperimentale (OGS), Italy

Reviewed by:
Cataldo Godano, University of Campania Luigi Vanvitelli, Italy
Prosanta Kumar Khan, Indian Institute of Technology Dhanbad, India

****Correspondence:***
A. A. Baranov
baranov@ifz.ru

Specialty section:
This article was submitted to Solid Earth Geophysics, a section of the journal Frontiers in Earth Science

Received: *06 May 2020*
Accepted: *26 October 2020*
Published: *21 December 2020*

Citation:
Shebalin PN and Baranov AA (2020) Aftershock Rate Changes at Different Ocean Tide Heights. Front. Earth Sci. 8:559624. doi: 10.3389/feart.2020.559624

INTRODUCTION

During last decades, the question of the effect of ocean tides on seismicity has been widely investigated. The issue of whether tidal forces really affect seismicity has been raised many times in the literature. Most of the studies established a connection between tides and seismicity, mainly on a regional scale (Klein, 1976a; Klein, 1976b; Souriau et al., 1982; Wilcock, 2001; Lin et al., 2003; Tanaka et al., 2004; Crockett et al., 2006; Stroup et al., 2007; Tanaka, 2010; Chen et al., 2012a; Datta and Kamal, 2012; Tanaka, 2012; Ide and Tanaka, 2014; Saltykov, 2014; Vergos et al., 2015; Arabelos et al., 2016; Baranov et al., 2019; Scholz et al., 2019) and others. There are also many studies linking seismicity and tides using global catalogues (Heaton, 1975; Nikolaev, 1994; Tsuruoka, et al., 1995; Tanaka et al., 2002; Cochran et al., 2004; Yurkov and Gitis, 2005; Métivier, et al., 2009; Chen et al., 2012b; Ide et al., 2016). However, many studies do not find such a correlation (Schuster, 1897; Morgan et al., 1961; Knopoff, 1964; Simpson, 1967; Shudde and Barr, 1977; Heaton, 1982; Rydelek et al., 1992; Vidale et al., 1998). A detailed review of the influence of tides on seismicity was given, for example, in (Emter, 1997).

Laboratory experiments were also conducted to study the effect of tides on seismicity (Lockner and Beeler, 1999; Beeler and Lockner, 2003). A strong correlation was found to exist between periodic stress (tides) and the occurrence of failure (earthquake) at shear stress amplitudes above approximately 0.3 MPa. Shear stress variations between 10 kPa (1 m of ocean tide load) and 0.1 MPa represent a transition region in which correlation with earthquake occurrence may occur. For amplitudes below 10 kPa (the order of the vertical component of the Earth tide), little or no correlation can be detected. These results are consistent with observations. This suggested that tidal stress amplitudes of about 3–10 kPa are required to trigger earthquakes (Hardebeck et al., 1998; Cochran et al., 2004). For example, it was shown that aftershocks after the M = 7.4 Landers event were triggered by stress increases greater than 10 kPa (Stein, 1999).

Largely since (Schuster, 1897), the tidal phases, mainly the semidiurnal phase, were studied. The amplitude-frequency properties of tides are very complex, and it is necessary to take into account the change in the amplitudes of various components of the tides. However, some studies such as (Klein, 1976a; Klein, 1976b; Souriau et al., 1982; Vidale et al., 1998; Lockner and Beeler, 1999; Wilcock, 2001; Beeler and Lockner, 2003; Stroup et al., 2007) and more recent ones (Ide and Tanaka, 2014; Ide et al., 2016; Baranov et al., 2019) analyzed tidal heights rather than tidal phases. The present study is concerned with aftershock rates after large earthquakes. This gives us high rates and high rate changes on the time scale of hours and days, compatible with the time scale of tides. In this time scale, tide height analysis seems more appropriate due to the complex tide phase structure. Actually, researchers studied the effect of Earth tides (Morgan et al., 1961; Heaton, 1975; Klein, 1976a; Klein, 1976b; Heaton, 1982; Burton, 1986; Rydelek et al., 1992; Lin et al., 2003; Métivier et al., 2009; Chen et al., 2012a; Chen et al., 2012b; Datta and Kamal, 2012; Saltykov, 2014) or the combined effect of Earth and ocean tides on seismicity (Souriau et al., 1982; Vidale et al., 1998; Tsuruoka, et al., 1995; Wilcock, 2001; Tanaka et al., 2002; Tanaka et al., 2004; Cochran et al., 2004; Stroup et al., 2007; Tanaka, 2010; Tanaka, 2012; Ide et al., 2016).

There are relatively few studies where the connection between seismicity and ocean tides was analyzed. This is due to the complexity of numerical calculations of ocean tides. Only in recent years computer programs for the numerical modeling of ocean tides have been developed. These programs were used to study the connection between ocean tides and seismicity (Crockett et al., 2006; Ide and Tanaka, 2014; Baranov et al., 2019). The result was to detect a clear connection between seismicity and ocean tides. Despite a large number of comparative studies of seismicity and tides, the relationship between aftershock rates and tides was studied in few papers (Souriau et al., 1982; Chen et al., 2012b; Datta and Kamal, 2012; Saltykov, 2014; Baranov et al., 2019). A partial dependence of aftershock rate on tidal heights (ocean and Earth tides) for normal-fault and thrust-fault earthquakes was found for the Pyrenees (Souriau et al., 1982). But for strike-slip earthquakes no statistical connection was found. The M >7 earthquakes worldwide since 1900 are more likely to occur during the 0°, 90°, 180° or 2,70° phases (i.e., earthquake-prone phases) of the semidiurnal solid Earth (M_2) tidal curve (Chen et al., 2012b). Diurnal and semi-diurnal periodicities in aftershock rate ($M \geq 4$) were found for the aftershock sequence of the Tohoku M = 9.1 earthquake of March 11, 2011 in Japan with an apparent weakening of the tidal triggering effect over time (Datta and Kamal, 2012). This suggests that large aftershocks in the fault zone of the Japan 2011 earthquake were strongly influenced by Earth tides.

Partial dependence of aftershock rates on Earth tides was also found for aftershocks of the M = 6.8 earthquake of June 21, 1996 off Kamchatka (Saltykov, 2014), and an alternative trigger mechanism was proposed for tidal effects based on an amplitude-dependent dissipation model. Another study of aftershock sequences following Kamchatka earthquakes using the method of differential probability gain, DPG (Baranov et al., 2019), demonstrated a considerable increase in the aftershock rate (by factors of two and more) at low or at high water. An increase in aftershock rate at low water corresponds to unloading of the seafloor, while high water may result in an increase of pore pressure in the fracture zone and therefore decreasing friction forces. The correlation between seismicity and tides in relation to focal mechanisms was studied by several authors. Correlation was mainly found for normal and partly for thrust slip types (Heaton, 1975; Souriau et al., 1982; Tsuruoka, et al., 1995; Tanaka et al., 2002; Cochran et al., 2004). The connection between seismicity and tides at ocean ridges were studied extensively (Wilcock, 2001; Tolstoy et al., 2002; Stroup et al., 2007; Scholz et al., 2019). A correlation between tides and seismicity was found along the Juan de Fuca Ridge (Wilcock, 2001; Tolstoy et al., 2002) and for East Pacific Rise (Stroup et al., 2007). Scholz et al. (2019) suggested pulsation of magma chambers due to vertical stress changes as a mechanism responsible for the tidal triggering of earthquakes for mid-ocean ridges.

The impact of tides on earthquakes is often explained by changes in the stress field in the fault using the Coulomb criterion (Stein, 1999; Cochran et al., 2004). Coulomb failure stress change $\Delta\tau_c = \Delta\tau + \mu(\Delta\sigma_n - \Delta P)$, where τ and σ_n are the shear stress change on the fault (assumed to be positive in the direction of slip) and the normal stress change on the fault (positive if the fault is unclamped), respectively, P is the pore pressure change in the fault, and μ is the coefficient of friction (with range 0–1). Failure is encouraged if $\Delta\tau_c$ is positive and discouraged if negative; both increased shear and unclamping of faults facilitate failure. Thus friction threshold can be exceeded either when the normal stress is decreased or when pore pressure is increased (Klein, 1976a; Klein, 1976b; Wilcock, 2001; Tolstoy et al., 2002; Cochran et al., 2004; Stroup et al., 2007; Métivier et al., 2009). This can reflect earthquake initiation (Stein, 2004). Some authors suggested alternative mechanisms to explain the effect of tides on seismicity: nonlinear dilatancy-diffusion model (Heaton, 1982), seismic modulation by combination of different tidal waves, impacts of tidal waves occurring in resonance with the self-oscillating system of the focal zone under the influence of tidal waves (Nikolaev, 1996) or an amplitude-dependent dissipation model taking into account tidal variations in physical properties

TABLE 1 | A review of studies of the impact of tides on seismicity.

№	Paper	Earth tides	Ocean tides	Tidal phase	Connection with seismicity	Tidal amplitude	Influence mechanism, methods	Object of investigations
1	(Morgan et al., 1961)	+	–	–	–	–	No definite evidence for effects due to earth tides	1933 earthquakes from different regions
2	(Heaton, 1975)	+	–	+	+ Partly. Oblique slip and dip-slip earthquakes are triggered by tidal stresses, M > 5, depth <30 km	–	Tidal triggering is discussed from the viewpoint of the dilatancy-diffusion model. The earthquake frequency is highest with tidal phase from –90° to 90°	107 earthquakes from different regions
3	(Klein, 1976a)	+	–	+	+ Partly	+ Through vertical stress	Three conceivable triggering mechanisms: Maximum shear stress, least compressive normal stress and maximum pore pressure	Mainshocks and aftershocks (M > 5), mid-atlantic ridge and Iceland region
4	(Klein, 1976b)	+	–	+	+ Partly	+ Through vertical stress	Tidal stresses are oriented to enhance the tectonic stress. No preference between elastic loading and pore pressure as the mechanism of reservoir-induced seismicity. The time of primary earthquake occurrence is mostly during the quarter of the tidal cycle in which tidal shear stress most enhances fault slip	Eight reservoirs, 10–20 mainshocks for each reservoir
5	(Heaton, 1982)	+	–	+	–	–	Dilatancy-diffusion model for tidal triggering	328 earthquakes from different regions
6	(Souriau et al., 1982)	+	+	+	+ Partly, for normal and thrust fault types	+	Statistical test using binomial distribution. Model takes into account both phase and amplitude variations of the tidal stresses	Aftershock sequence in the pyrenees (515 events)
7	(Burton, 1986)	+	–	–	+ Partly	–		An overview
8	(Rydelek et al., 1992)	+	–	+	– The results of the schuster test indicate lack of tidal triggering	–	Tidal stress may trigger an earthquake by increasing the shear stress, by decreasing the effective normal stress, or by some combination of these factors	Earthquake swarms, Pozzuoli catalogue, Italy
9	(Nikolaev, 1994)	+	–	+	+ Partly for some areas	–	No mechanism	Hadson`s catalogue from 1962 to 1988, M > 5
10	(Tsuruoka, et al., 1995)	+	+	+	+ Partly for normal fault, maximum seismicity for tidal phase from 0° to 60° –For strike-slip or thrust	–	Normal-fault-type earthquakes tend to occur at the time when the cubic tidal stress takes a maximum tensile value or a little bit later	988 globally distributed earthquakes with magnitude of 6.0 or larger from CMT from 1977 to 1992
11	(Nikolaev, 1996)	+	–	+	+ Partly, for some areas	–	Two possible mechanisms: Seismic modulation by combination of different tidal waves or hit in resonance of the self-oscillating system of the focal zone under the influence of tidal waves	8,985 events for caucasus, 3 < M < 5.5, 1962–1989; Hadson`s catalogue, 8,500 events, 1962–1988 without aftershocks
12	(Hardebeck et al., 1998)	–	–	–	+ Partly	–	Static stress change triggering model is useful in explaining the landers aftershocks particularly those which are not too close to (d < 5 km or [ACS> 0.5–1 MPa]) or too far from (d > 75 km or [ACS <0.01 MPa]) the mainshock fault plane	California, 2 aftershock sequences from landers and northridge earthquakes
13	(Vidale et al., 1998)	+	+	+	–	+ Through vertical stress	Probability distribution of tidal stress. Binomial model of triggering	13,042 earthquakes near San-Andreas fault (1969–1994)

(Continued on following page)

TABLE 1 | (*Continued*) A review of studies of the impact of tides on seismicity.

№	Paper	Earth tides	Ocean tides	Tidal phase	Connection with seismicity	Tidal amplitude	Influence mechanism, methods	Object of investigations
14	(Lockner and Beeler, 1999)	–	–	–	–	+ Through vertical stress	Strong correlation between the periodic stress and the occurrence of failure at shear stress amplitudes above approximately 0.3 MPa. Little or no correlation at amplitudes below 0.01 MPa	Laboratory experiments. Samples were deformed in a triaxial loading frame at constant confining pressure 50 MPa. Earth's crust permits delayed failure
15	(Wilcock, 2001)	+	+	+	+ The earthquake frequency nearly doubles at the lowest tides	+ Frequency of events as a function of tidal height	The earthquake frequency is lowest at high water and highest at low water and in the quadrant following low water	1899 microearthquakes recorded during a 55 days experiment on the endeavor segment of the Juan de Fuca ridge
16	(Tanaka et al., 2002)	+	+	+	+ Partly	–	Correlation is found for reverse fault type and normal fault type. Earthquakes tend to occur when the tidal stress accelerates the fault slip. There is no correlation for strike-slip type	9,350 global events from CMT, M > 5.5
17	(Tolstoy et al., 2002)	+	+	–	+ Maximum at low water	+	Reduction in normal stress, which causes faults already very close to their failure point to slip, increasing of pore pressure. Schuster`s test	402 earthquakes near the summit caldera of axial volcano on the Juan de Fuca ridge
18	(Lin et al., 2003)	+	–	+	+ Partly, correlation only for 2.5 < M < 5	–	No mechanisms	1973–1991 local Taiwan catalogue
19	(Beeler and Lockner, 2003)	–	–	–	+ Partly for earth tides, minimum 13,000 earthquakes are needed	+ Through vertical stress	Delayed failure is key to understanding why earthquake occurrence correlates weakly with small stress changes such as the solid earth tides	Laboratory experiments. The degree of correlation between failure time and the phase of the driving stress depends on the amplitude and frequency of the stress oscillation and on the stressing rate
20	(Saltykov et al., 2004)	+	–	+	+ Before mainshock in focal area	–	No mechanism, maximum of seismicity for positive values of the decreasing tidal height with a delay to a quarter of the period concerning a maximum	Catalogue of Kamchatka, M > 2.6, only mainshocks
21	(Tanaka et al., 2004)	+	+	+	+ Partly	–	Earthquakes preferentially occur when the tidal compressional stress is near the dominant direction of P-axes of focal mechanisms obtained in the corresponding regions	Japan meteorological agency for the period from October 1997 to May 2002, they use the origin times and hypolefts of shallow earthquakes (focal depth ≤70 km, M ≥ 2.0) occurring in Japan
22	(Cochran et al., 2004)	+	+	+	+ Partly	–	Earthquake triggering correlation is found for coefficient of friction between 0.2 and 0.6, using binomial and Schuster`s tests	Only main events (2027) from CMT, depth 0–40 km, M > 5.5
23	(Yurkov and Gitis, 2005)	+	–	+	+	–	Only lunar forces investigated, standard statistical test only	National Earthquake Information Center (NEIC) catalogue 161,060 earthquakes, M > 4, 1973–1999
24	(Crockett et al., 2006)	–	+	+	+	–	December 26, 2004 sumatra earthquake and its principal aftershocks (20–30 km depth) occurred in close relation to new and full moons	December 26, 2004 sumatra earthquake and its aftershocks. Advanced national seismic system database (www.ncedc.org/anss). 5,807 earthquakes of m_b = 3.5 and greater. Ocean tides were calculated using JTides program
25	(Stroup et al., 2007)	+	+	+	+ Maximum at low water	+ Tidal height	The modulation of 9°50′N microearthquakes by small-amplitude periodic stresses is consistent with earthquake nucleation within a high stressing rate environment that is maintained near a critical state of failure by on-axis magmatic and hydrothermal processes	Microearthquakes at 9°50′N East pacific rise

(Continued on following page)

TABLE 1 | (*Continued*) A review of studies of the impact of tides on seismicity.

№	Paper	Earth tides	Ocean tides	Tidal phase	Connection with seismicity	Tidal amplitude	Influence mechanism, methods	Object of investigations
26	(Métivier et al., 2009)	+	–	+	+ Clear correlation (with ~99% confidence) between the phase of the solid earth tide and the timing of seismic events	–	Earthquakes occur slightly more often at the time of ground uplift by the earth tide. No evidence for a focal mechanism dependence on earthquake triggering. Tidal stresses trigger up to about 0.2–0.3% of all the earthquakes. Shallow earthquakes are more easily triggered, because tidal dilations become relatively smaller	The NEIC catalogue with 442,412 events 1973–2007, M > 2.5
27	(Tanaka, 2010)	+	+	+	+	-	The frequency distribution of tidal phase angles in the prevent period before mainshock exhibited a peak near the angle where the tidal shear stress is at its maximum to accelerate the fault slip	Tidal triggering of earthquakes precursory to the three giant earthquakes (December 26, 2004, M = 9.0, March 28, 2005 M = 8.6, and September 12, 2007, M = 8.5). Global CMT catalogue, depth<70, 1976–2008, M > 5
28	(Chen et al., 2012a)	+	–	+	+ Maximum at low water	–	No mechanism, EMD statistical method, tidal triggering effect in both the non-declustered and declustered catalogues	Taiwan Telemetered Seismic Network catalogue earthquakes that occurred near Taiwan between 1973 and 2008
29	(Chen et al., 2012b)	+	–	+	+	–	M > 7 earthquakes are more likely to occur during the 0°, 90°, 180° or 270° phases of the semidiurnal solid earth tidal curve (M2)	420,747 M > 4 global earthquakes, aftershock sequence of the M = 6.2 Christchurch, New Zealand
30	(Datta and Kamal, 2012)	+	–	+	+	–	No mechanism	1,370 aftershocks (M > 4) during 1 month in the fault area of Japan earthquake of March 2011
31	(Tanaka, 2012)	+	+	+	+ Maximum seismicity for tidal phase from –90° to 90° before mainshock for focal area	–	Tidal phase distribution of earthquakes exhibits a peak where the shear stress is at its maximum to promote failure.No significant tidal correlation is found after the Tohoku-Oki mainshock	Focal area of Tohoku-Oki earthquake before main event (ten years) shallow earthquakes (depths less than 70 km) in the global CMT catalogue from 1976 to 2011, M > 5
32	(Ide and Tanaka, 2014)	–	+	+	+ Maximum seismicity at low water	+ Through shear stress	Strong correlation, most of events occur at low water from minimum to increasing of lithostatic pressure. A low water results in increased shear stress and decreased normal stress unclamping, resulting in an enhancement of plate subduction	Deep Tremor, western Japan, ocean tides were calculated using JTides program
33	(Saltykov, 2014)	+	–	+	+ Partly	–	An alternative trigger mechanism based on an amplitude-dependent dissipation model, taking into account tidal variations of the physical properties of a medium	147 aftershocks for (June 21, 1996, M = 6.8) event, Kamchatka
34	(Vergos et al., 2015)	+	+	+	+ Seismicity corresponds with the diurnal luni-solar (K1) and semidiurnal solar (S2) tidal variations	–	No mechanism, Schuster`s test	Catalogue of Geodynamic institute of the National Observatory of Athens (http://www.gein.noa.gr/services/cat.html), 16,137 shallow and 1,482 deep earthquakes with M < 6.2 occurred from 1964, to 2012, around the Hellenic Arch
35	(Arabelos et al., 2016)	+	+	+	+ Seismicity corresponds with the diurnal luni-solar (K1) and semidiurnal solar (S2) tidal variations	+	No mechanism, Schuster`s test	National Observatory of Athens catalogue, 33,281 shallow and 769 of intermediate depth earthquakes, Greece, 0.2 < M < 6.3, from January 1964 to December 2013, in an area bounded by $38^\circ \le f \le 39^\circ$ and $21^\circ \le \lambda \le 23^\circ$

(Continued on following page)

TABLE 1 | (*Continued*) A review of studies of the impact of tides on seismicity.

№	Paper	Earth tides	Ocean tides	Tidal phase	Connection with seismicity	Tidal amplitude	Influence mechanism, methods	Object of investigations
36	(Ide et al., 2016)	+	+	+	+ Partly, large earthquakes tend to occur near the time of maximum tidal stress amplitude	+ Through shear stress	Estimation of b-values and Utsu's test. The *b*-value decreases as the amplitude of tidal shear stress increases. The probability of a tiny rock failure expanding to a gigantic rupture increases with increasing tidal stress levels. Large earthquakes are more probable during periods of high tidal stress	CMT catalogue with M > 5.5 (>10,000 events, 1976–2015); National Research Institute for Earth Science and Disaster Resilience F-net moment tensor catalogue for earthquakes in northeastern Japan of Mw > 4.5, from 1997 to 2015; and the refined earthquake focal mechanism catalogue for southern California for earthquakes in southern California with M > 2.5
37	(Varga and Grafarend, 2017)	+	+	–	–	–	Triggering effect of earth tides is different in case of zonal, tesseral, and sectorial tides and also significantly depends on the latitude. Only the horizontal shear stresses produced by earth tides are most likely to influence the outbreak of an earthquake. The influence of load tides (ocean tides) is limited to the loaded area and its immediate vicinity	Theoretical model
38	(Baranov et al., 2019)	–	+	–	+	+ Tidal height	Mechanisms: Friction reduction in a fault due to vertical stress decreasing at low waters and increased pore pressure at high waters	16 aftershock sequences of earthquakes near Kamchatka with M > 6, depth<50 km from regional catalogue produced by the Geophysical survey of the Russian academy of sciences
39	(Scholz et al., 2019)	+	+	+	+	+	Tidal triggering of mid-ocean ridge seismicity, earthquakes occur preferentially during low water	Axial volcano on the Juan de Fuca ridge, ~60,000 earthquakes located between January 22nd and April 23rd, 2015

of the medium (Saltykov, 2014). The researchers used different methods to study the effect of tides on seismicity from simple visual comparison between time series of seismicity and tides to more or less sophisticated statistical methods as binomial distribution test, random distribution test, method of Chapman-Miller (Malin and Chapman, 1970), and Schuster's test using a statistical method of Rayleigh (Schuster, 1897). Schuster's test was described in detail in many papers (e.g., Heaton, 1975; Rydelek et al., 1992). **Table 1** summarized studies of tides on seismicity using several key parameters: type of tides (Earth tides, ocean tides), tidal phases, connection with seismicity, tidal amplitude, the mechanism responsible, and the object of study.

Why do we study the impact of ocean tides on aftershock rate using a model of tide heights?

(1) Time scales of tides and aftershock occurrence are comparable. The time-dependent distribution of aftershocks without impact of tides can be modeled.
(2) The impact of ocean tides on aftershock rates still remains a challenge (Cochran et al., 2004; Tanaka, 2012; Baranov et al., 2019).
(3) The well-known Schuster test using tide phases requires a correct catalogue declustering. Aftershocks that remain in the catalogue may alter the statistics.
(4) The impact of ocean tides on seismicity is often related to instabilities or a compliance of fault zones (Cochran et al., 2004). The aftershock zones marked by high stress perturbations perfectly fit those conditions.
(5) We concentrate here on ocean tides in areas where the amplitudes are 2 m or more (Kamchatka and New Zealand). The corresponding stress changes (10–20 kPa) are larger compared with Earth tides (Varga and Grafarend, 2017).
(6) We study ocean tide heights, not phases. Triggering of earthquakes is caused by stress changes depending on the level of tides. The frequency structure of the ocean tides is complex, and the prevailing periods may vary in time (Lyard et al., 2006).

The purpose of this publication is to assess the quantitative effect of ocean tidal heights on seismic activity and to compare these estimates for different types of faults.

METHODS

Selection of Aftershock Sequences

The aftershock sequences for analysis were found using the "nearest neighbor" algorithm of Zaliapin and Ben-Zion (Zaliapin and Ben-Zion, 2013). Aftershock sequences of large earthquakes may have complex structure, with significant "splashes" of secondary aftershocks caused by large primary aftershocks. Another component of seismicity is background seismicity, which is often referred to as seismic noise. Using the "nearest neighbor" algorithm, we selected only the direct "offspring" (Zaliapin and Ben-Zion, 2013) of the considered large earthquakes, thus minimizing the presence of secondary aftershocks and background seismicity in the selected sequences. This allowed us to model the aftershocks sequences using Omori's law. One alternative that we used in a previous analysis (Baranov et al., 2019) is the Molchan-Dmitrieva algorithm (Molchan and Dmitrieva, 1992), which selects aftershock sequences together with secondary aftershock subsequences. Large aftershocks often trigger a temporary increase of activity. In such cases the Omori model may be significantly altered by this temporary activation. Direct aftershocks found using the nearest neighbor approach do not contain the secondary aftershock sequences, and thus are correctly modeled by the Omori law. Another alternative could be a stochastic declustering of the earthquake catalogue with much deeper complexity and non-uniqueness of the clusters (Varini et al., 2020). Another disadvantage of the stochastic declustering methods is their basic hypothesis that the number of aftershocks

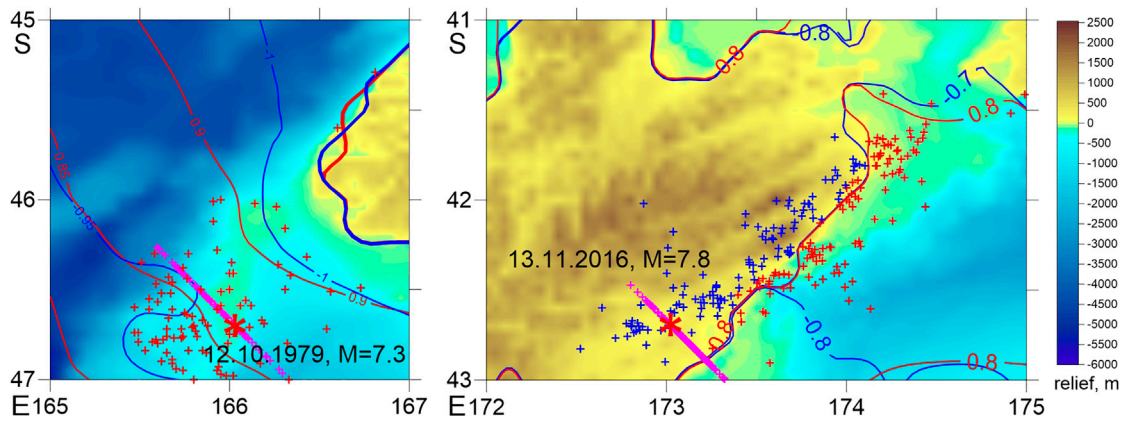

FIGURE 1 | Maps of tidal heights and examples of aftershock sequences in the interval (t_c, 720 h) of M = 7.3 earthquake of October 12, 1979, New Zealand **(A)** and M = 7.8 earthquake of November 13, 2016, New Zealand **(B)**. Crosses mark aftershock epicenters: red in the ocean, blue on land. Red contours show maximum ocean levels, whereas blue contours show minimum levels. Colour scale shows the relief (m) with respect to sea level.

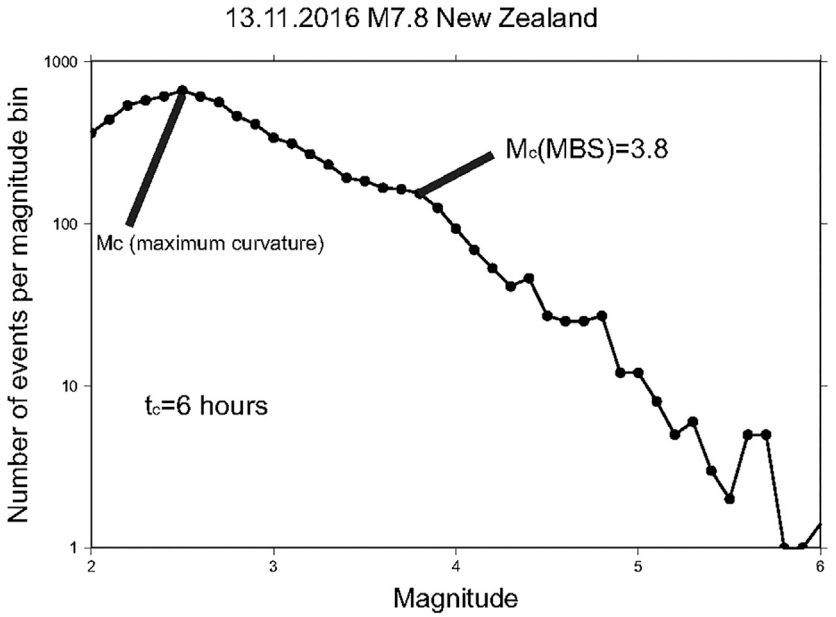

FIGURE 2 | Diagram of the magnitude of completeness M_c using data in the interval (t_c, 1 month) after the main shock (New Zealand, M = 7.8, November 13, 2016).

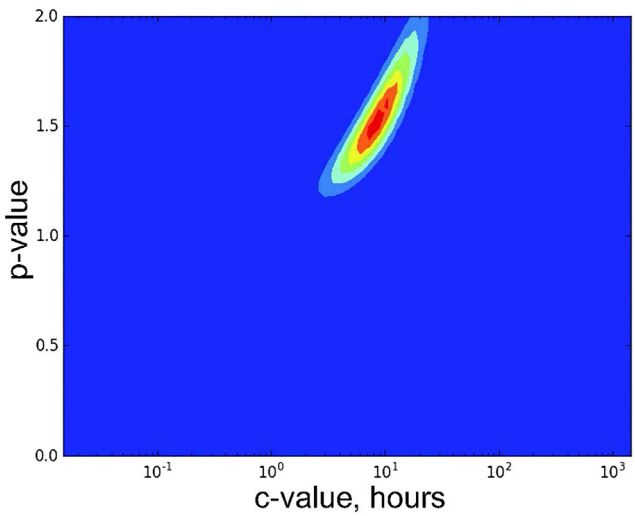

FIGURE 3 | The posterior distribution of the c and *p* values for Bayesian estimates (Holschneider et al., 2012) for aftershocks of the M = 7.8 earthquake of December 5, 1997 in Kamchatka. Light-blue area corresponds to the 95% quantile.

is a function of the magnitude of the corresponding main shock. This hypothesis, as was recently found, is not true (Shebalin et al., 2020).

We selected M ≥6 main shocks in the Kamchatka region, and M ≥6 events in the New Zealand region, which have offshore aftershocks. **Figures 1A,B** show a map of the maximum ocean tide amplitude with resolution 0.125° together with examples of offshore aftershocks for M = 7.5 (Kamchatka, June 08, 1993) and M = 7.8 (New Zealand, November 13, 2016) earthquakes. All aftershocks (as described above, we consider only direct aftershocks of the large earthquakes considered using the nearest neighbor approach), both onshore and offshore ones, were used to estimate the parameters of the Omori–Utsu law (Utsu, 1961), but only the offshore aftershocks were used to calculate the effects of ocean tides on seismicity. For selection of direct aftershocks in Kamchatka and New Zealand we used the parameters listed in **Supplementaty Table S1** of (Shebalin et al., 2020).

The Magnitude of Completeness Magnitude M_c and Time of Completeness t_c

The catalogue completeness usually decreases after large earthquakes (Helmstetter et al., 2006; Hainzl, 2016; Shebalin and Baranov, 2017). For each aftershock sequence we began by estimating the magnitude of completeness M_c using data in the interval (t_c, 1 month) after the main shock by the MBS method (Cao and Gao, 2002; Wossner and Wiemer, 2005) and t_c = 1 h. At this stage we disregarded data within first 6 h after the main shocks, where which the catalogue usually remains incomplete even for relatively large magnitudes. The MBS method allows one to detect the frequently observed effect of the lack of low-magnitude aftershocks during the first few hours and sometimes days after a large earthquake, not detectable by the Maximum Curvature technique (Wiemer and Wyss, 2000), see the example in **Figure 2**. Then, with the preliminary value of M_c, we found t_c using the equation (Helmstetter et al., 2006) $M_c = M_m - 4.5 - 0.75 \log_{10}(t_c)$, where M_m is the mainshock magnitude. The next step was to find the final value M_c using the same MBS technique, but with the new value of t_c. In the

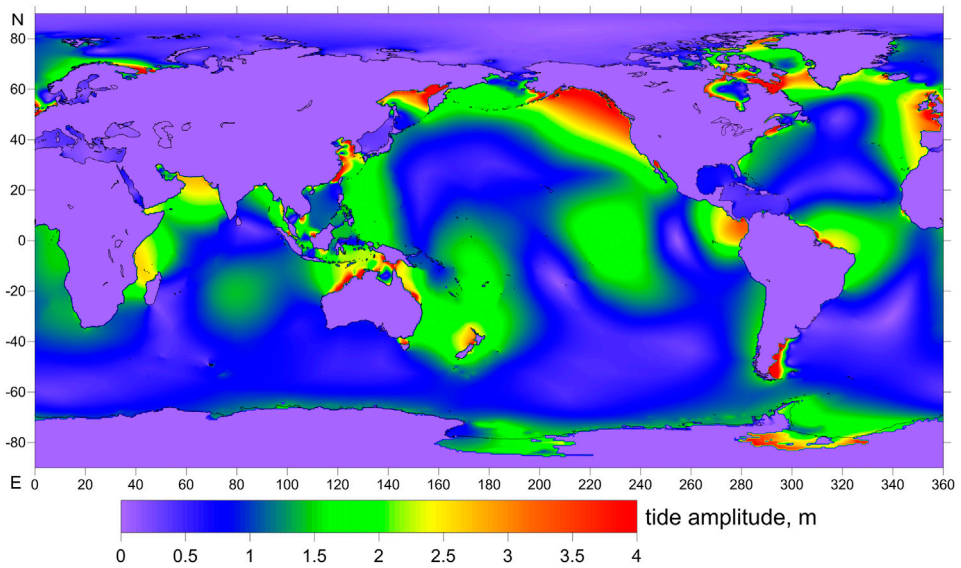

FIGURE 4 | A global map of ocean tide amplitude. The colour scale shows the maximum amplitude of the ocean tide, m.

following analysis we omit the interval $(0, t_c)$ after the main shocks.

Modelling the Aftershock Rates

We model aftershock rates $\lambda(t)$ using the Omori-Utsu model (Utsu, 1961)

$$\lambda(t) = \frac{K}{(t+c)^p}$$

where t is the time after the main shock, and c, p, and K are parameters. We estimated the parameters using aftershocks with $M \geq M_c$ in an interval (t_c, 720 h) with the Bayesian approach (Holschneider et al., 2012), assuming that c and p are homogeneous. **Figure 3** shows an example of the posterior distribution of (c, p) Bayesian estimates. We subdivide the aftershock zone into 0.2° × 0.2°boxes. The interval (t_c, 720 h) is divided in subintervals of 0.2 h. Supposing the c-value and the p-value are equal in all boxes, we calculated the modeled rates of

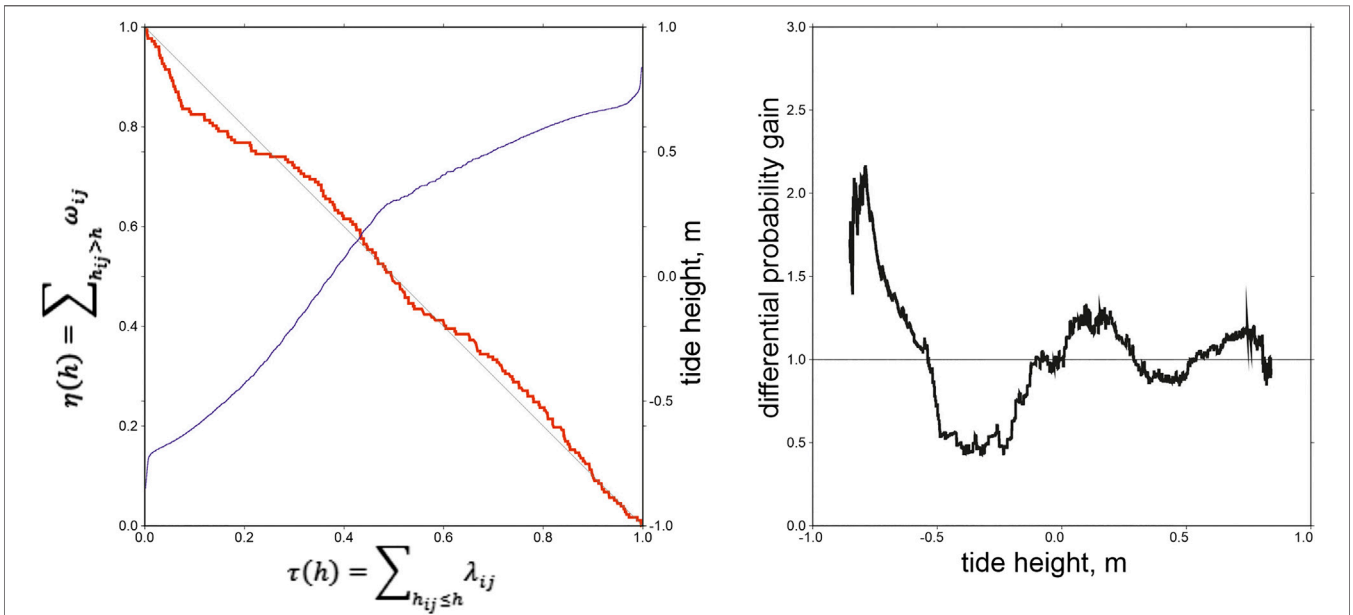

FIGURE 5 | An example of the differential probability gain function. Aftershocks of the M = 6.3 earthquake of June 21, 1992 in New Zealand. **A)** Error diagram (red line), $\eta(h) = \eta(\tau(h))$, with $\tau(h) = \sum_{h_{ij} \leq h} \lambda_{ij}$, $\eta(h) = \sum_{h_{ij} > h} \omega_{ij}$. The diagonal line $\eta = 1 - \tau$ corresponds to no impact ($\omega_{ij} = \lambda_{ij}$), blue line shows inverse function $h(\tau)$. **(B)** Differential probability gain function. Its values correspond to the slope of the error diagram as a function of h as given by **Eq. 2**.

TABLE 2 | The main parameters of the aftershock sequences for Kamchatka region. *H* denotes the main shock depth of focus; *M* is the mainshock magnitude; *N* denotes the number of $M \geq Mc$ aftershocks in the interval (t_c, 720 h) measured from the main shock time; the maximum amplitude of ocean tide in the interval (t_c, 720 h) measured from main shock time was converted to pressure, kPa; ocean depth at the epicentre of main event, m; type indicates the focal mechanism of the main event.

№	Date of main shock	*H*, km	*M*	M_c	t_c, *hour*	*N*	p	c, hour	Max amplitude of ocean tide, kPa	Ocean depth, m	Type
1	December 15, 1971	20	7.8	3.5	12	114	1.02	32.5	19	1,740	?
2	February 28, 1973	59	7.5	4.0	1	54	0.98	1.63	13	1,500	?
3	December 28, 1984	19	6.7	4.0	1	31	0.98	0.33	16	215	Normal fault
4	July 10, 1987	49	6.3	3.5	1	55	0.70	0.40	19	6,000	Strike-slip
5	March 02, 1992	20	6.8	3.3	1	65	1.14	0.89	14	1,075	Thrust
6	June 08, 1993	40	7.5	3.5	3	176	1.23	8.04	15	160	Thrust
7	November 13, 1993	40	7.0	3.5	0.1	69	0.89	0.73	16	1,370	Thrust
8	December 05, 1997	10	7.8	3.3	2	273	0.70	2.42	16	3,060	Thrust
9	December 05, 1997	24	6.4	3.3	1	78	0.63	0.05	16	3,190	Thrust
10	March 08, 1999	7	6.9	3.2	1	94	1.11	0.89	10	3,260	Thrust
11	October 08, 2001	24	6.3	3.4	2	100	1.36	2.43	13	1,360	Thrust
12	March 15, 2003	5	6.0	3.2	1	74	1.02	0.49	14	4,170	Normal fault
13	December 05, 2003	29	6.6	3.3	2	102	1.11	2.96	17	3,120	Thrust
14	July 30, 2010	38	6.3	3.4	1	37	1.14	0.33	13	3,200	Thrust
15	February 28, 2013	61	6.8	3.5	1	39	0.79	0.27	13	650	Thrust
16	March 24, 2013	48	6.0	3.4	1	26	1.01	0.07	12	5,650	Normal fault

the aftershocks λ_{ij}, where i is the index of spatial box, and j the time subinterval:

$$\lambda_{ij} = A_i \int_{t_c+0.2j}^{t_c+0.2j+0.2} \frac{1}{(t+c)^p}\, dt \qquad (1)$$

where $A_i = \frac{N_i}{\int_{t_c}^{720} \frac{1}{(t+c)^p} dt}$, N_i is the actual number of aftershocks in the ith bin within the interval (t_c, 720 h). We calculated the actual number of aftershocks λ_{ij} in each spatio-temporal volume. **Figure 3** shows an example of the *p*-value diagram for the M = 7.8, Kamchatka, December 05, 1997 earthquake.

Modeling Tide Heights

Real ocean tides can be as high as 12–18 m in some bays. The tidal amplitudes can reach 2 m near the Pacific coast of Kamchatka and the coast of New Zealand, producing a pressure contrast of approximately 20 kPa. The elastic response of the solid Earth to the ocean load is obtained by convolution of seawater mass distribution using FES 2004 program (http://www.aviso.altimetry.fr/). FES 2004 gives tide height at a specified point at a specified time instant (Lyard et al., 2006). The program is based on the solution of tidal barotropic equations by finite elements (triangles) on a global element grid (~1 million elements). It uses numerical models of ocean bottom topography and shoreline (Le Provost et al., 1994; Le Provost et al., 1998). The program can compute 15 main tidal components on a 1/8° grid (amplitudes and phases), as well as 28 additional tidal components. The presence of ice is incorporated for polar regions. The accuracy is within a few centimeters for open ocean and within 10 cm for offshore areas. The grid is not uniform, being denser near the shore and less detailed in the open ocean, according to Le Provost's criterion (Le Provost and Vincent, 1986). The program requires an input file that contains site coordinates and times in hours as measured from January 1, 1985. The program uses the sites as specified in the input file to yield tide heights at a required time instant. If a point is on land, the value is −9999. Using the FES 2004 software we modelled the heights h_{ij} of the ocean tides in each spatio-temporal volume. Next, we built a map of maximum amplitudes of ocean tides for the entire world. This map was calculated using a program of our own, *Amplitude*. The program iterates over the coordinates of latitude and longitude at steps of 0.125°. For each point of the mesh, the program generates a time series for a year with time step 1 min. Then, for each time series, the FES 2004 program is launched, which calculates the tide height at a given point for the annual interval and finds the maximum tide amplitude at the point. Thus, a grid is obtained where for each point the maximum amplitude of ocean tide is found. **Figure 4** shows the map of the maximum ocean tide amplitude with resolution 0.125° for the entire world. New Zealand and Kamchatka that we deal with here are regions with large ocean tide amplitudes.

Differential Probability Gains

The ocean tide height can be considered as a parameter controlling the relative changes of seismicity rates. If a correlation between ocean tides and seismicity rates exists, then it is possible to calculate what is the average change of the rates relative to an average model, at specific values of the control parameter (**Figure 5A**). The differential probability gain (DPG) function (Shebalin et al., 2012; Shebalin et al., 2014) is defined as the ratio of the actual number of seismic events to the number expected on the average model. It is a function of the control parameter. Here we estimate a smoothed differential probability gain function g(h) using ranges of the control parameter with constant width *dh*:

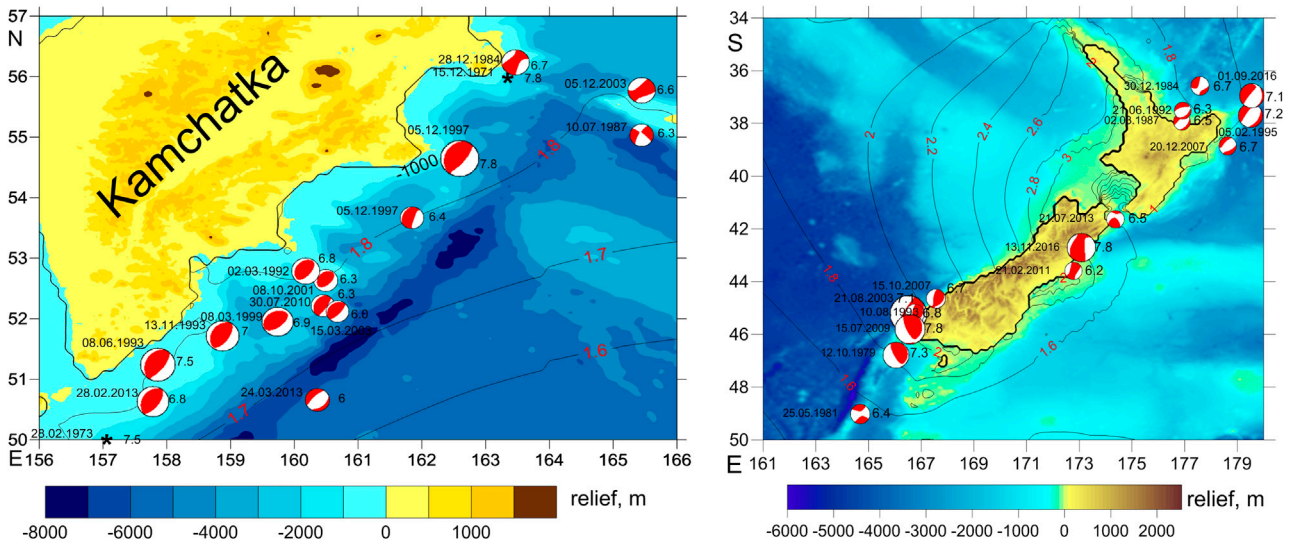

FIGURE 6 | Maps of $M \geq 6$ main shocks for Kamchatka, 1971–2013 **(A)** and New Zealand, 1979–2016 **(B)**. The colour scale shows the relief (m) with respect to sea level; black contours with red labels show maximum amplitude of the ocean tide, m. The mainshock fault-plane solutions were taken from the Global Centroid-Moment-Tensor catalogue (Ekström et al., 2012); epicentres prior to 1976 are not reported in Global Centroid-Moment-Tensor, and they are marked by asterisks.

TABLE 3 | The main parameters of the aftershock sequences for New Zealand. *H* denotes the mainshock depth of focus; *M* is the mainshock magnitude (magnitude M_L as converted from energy class in **Table 2**); *N* denotes the number of $M \geq M_C$ aftershocks in the interval (t_c, 720 h) measured from the mainshock time; the maximum amplitude of ocean tide in the interval (t_c, 720 h) measured from mainshock time was converted to pressure, kPa; relief at the epicentre of main event (m) with respect to sea level; type indicates the focal mechanism of the main event.

№	Date of main shock	*H*, km	*M*	M_c	t_c, hour	*N*	p	c, hour	Max amplitude of ocean tide, kPa	Relief (m) with respect to sea level	Type
1	October 12, 1979	12	7.3	3.8	1	81	0.92	0.33	18	−900	Thrust
2	May 25, 1981	33	6.4	4.2	0.1	55	1.20	1.99	15	−2,540	Strike-slip
3	December 30, 1984	12	6.7	4.0	1	76	0.92	0.60	18	−2,460	Strike-slip
4	March 02, 1987	10	6.5	3.3	2	125	1.30	1.89	19	20	Normal fault
5	June 21, 1992	5	6.3	3.2	1	133	1.49	2.09	20	−470	Normal fault
6	August 10, 1993	5	6.8	3.1	2	632	1.11	1.98	22	−2,200	Thrust
7	February 05, 1995	12	7.2	3.9	2	356	1.17	2.96	16	−2,500	Normal fault
8	August 21, 2003	24	7.1	3.5	2	375	1.14	1.63	21	−4,070	Thrust
9	ctober 15, 2007	5	6.7	3.3	6	89	1.36	6.58	22	−1,350	Thrust
10	December 20, 2007	33	6.7	3.5	1	29	0.82	0.60	16	−1,040	Normal fault
11	July 15, 2009	12	7.8	3.8	0.1	359	1.14	1.33	22	500	Thrust
12	February 21, 2011	5	6.2	3.2	1	295	0.98	0.49	20	60	Normal fault
13	July 21, 2013	16	6.5	3.2	2	184	1.20	2.09	18	−90	Strike-slip
14	September 01, 2016	22	7.1	3.2	3	323	1.17	5.39	20	−2,350	Normal fault
15	November 13, 2016	15	7.8	3.8	5	188	1.14	8.79	17	230	Thrust

$$g(h) = \frac{\sum_{i,j;h-dh<h_{ij}\leq h+dh}\omega_{ij}}{\sum_{i,j;h-dh<h_{ij}\leq h+dh}\lambda_{ij}} \quad (2)$$

Here, ω_{ij} and λ_{ij} denote, respectively, the actual numbers of seismic events and the numbers that are expected on the average model in spatial box i and time span j. The ocean tide height h may also be considered as an alarm function of a forecasting model. The error diagram (Molchan, 1991) evaluates retrospectively the performance of the model with respect to the reference model. With the error diagram (**Figure 5A**), the differential probability gains are defined as the local slope (derivative) of the diagram (**Figure 5B**). Thus we assume that at each point of the considered area and at any moment, a specific tide height corresponds to an increase or a decrease of the aftershock rate with respect to the local rate that would have been observed without the impact of tides. We model this

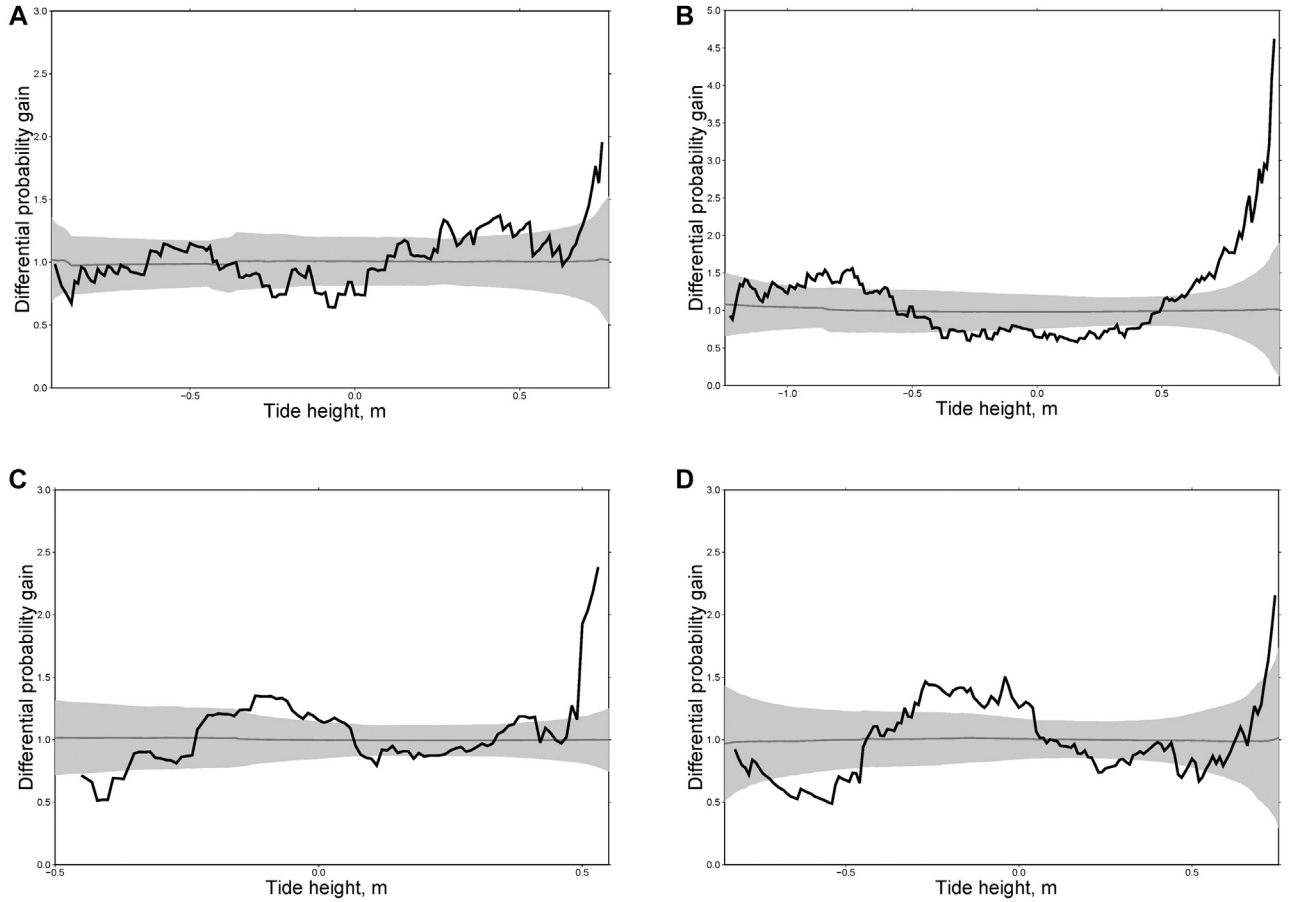

FIGURE 7 | Differential probability gain functions for four aftershock sequences for Kamchatka following the earthquakes of M = 6.7, December 28, 1984 **(A)**; M = 6.3, July 10, 1987 **(B)**; M = 6.8, March 2, 1992 **(C)**; M = 6.8, February 28, 2013 **(D)**. Solid line shows values of g, the straight line marks the level 1.0.

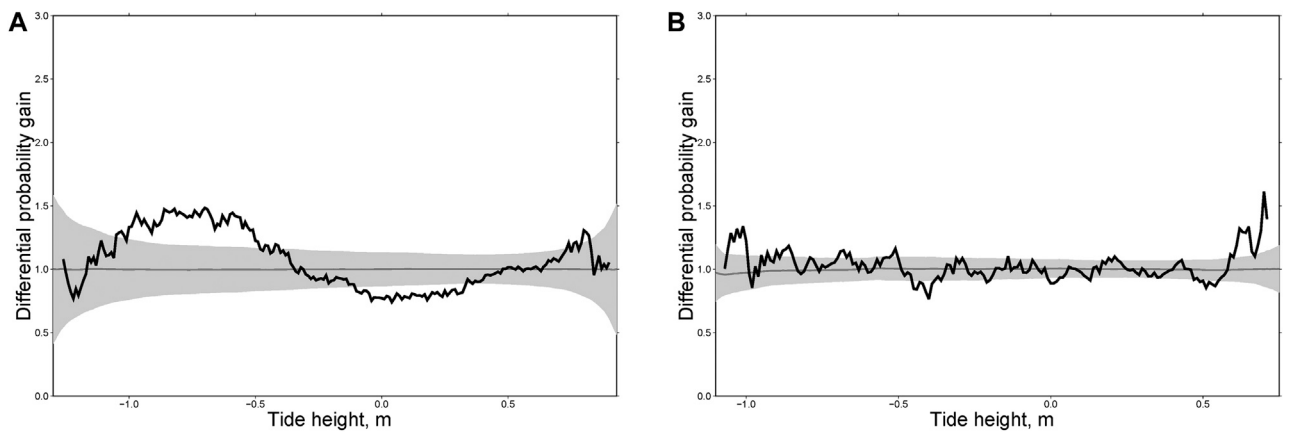

FIGURE 8 | Differential probability gain functions for two aftershock sequences in Kamchatka following the earthquakes of M = 7.8, December 15, 1971 **(A)** and M = 7.8, December 5, 1997 **(B)**.

expected tide-independent aftershock rate by the Omori-Utsu law in time with a spatial distribution obtained by averaging over two months, as defined by **Eq. 1**. The function g(h) is the corresponding indicator of influence. The larger the difference between *g(h)* and 1, the more significant is this impact at corresponding values of the ocean tide height *h*.

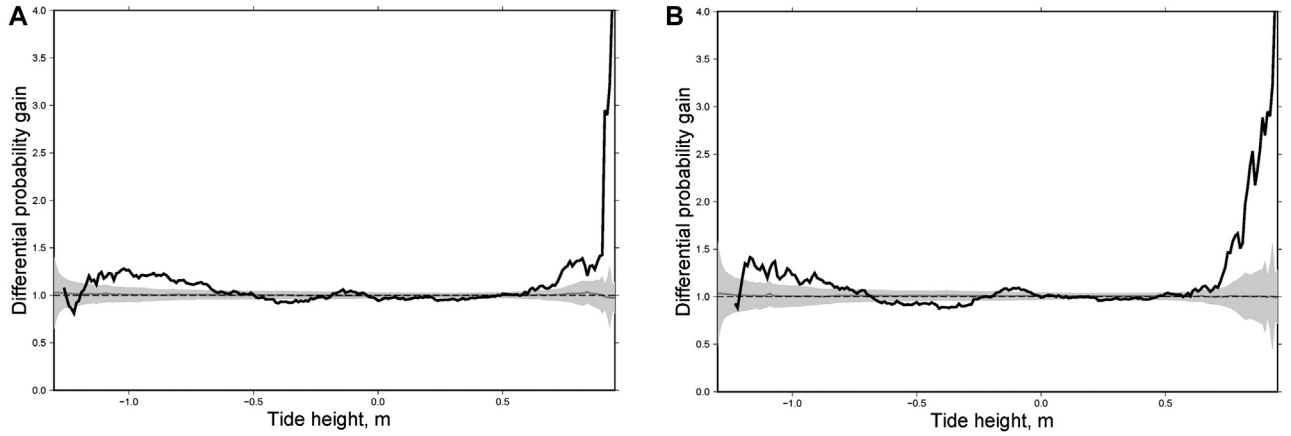

FIGURE 9 | Integral differential probability gain function for Kamchatka: all 16 aftershock sequences **(A)** and 14 sequences without those for the M = 7.8, December 15, 1971 and M = 7.8, December 5, 1997 earthquakes **(B)**.

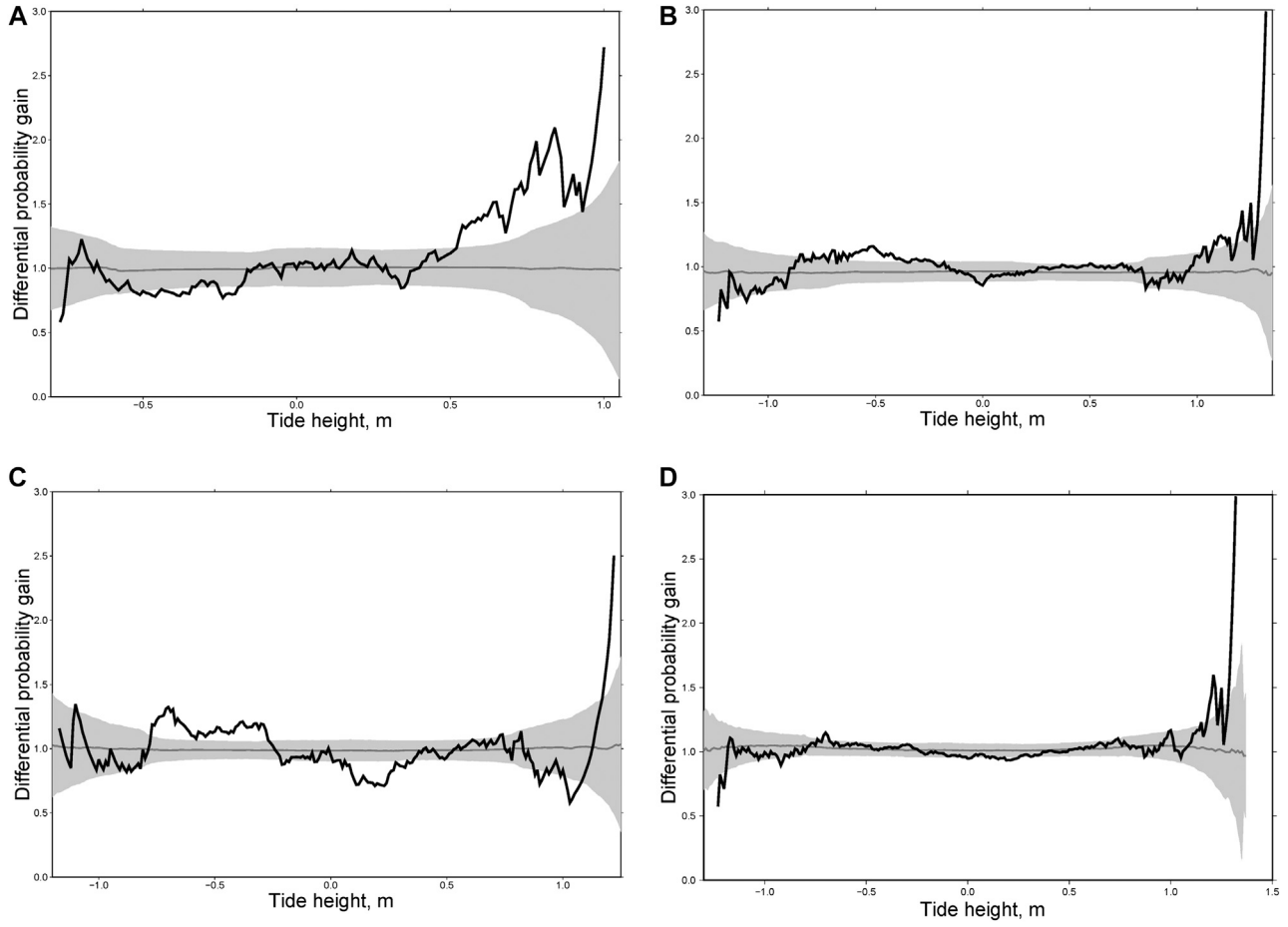

FIGURE 10 | Differential probability gain functions for three aftershock sequences in New Zealand following the earthquakes of M = 7.3, October 12, 1979 **(A)**; M = 6.8, August 10, 1993 **(B)**; M = 7.8, July 15, 2009 **(C)** and the integral differential probability gain function for five aftershock sequences of thrust type earthquakes **(D)**.

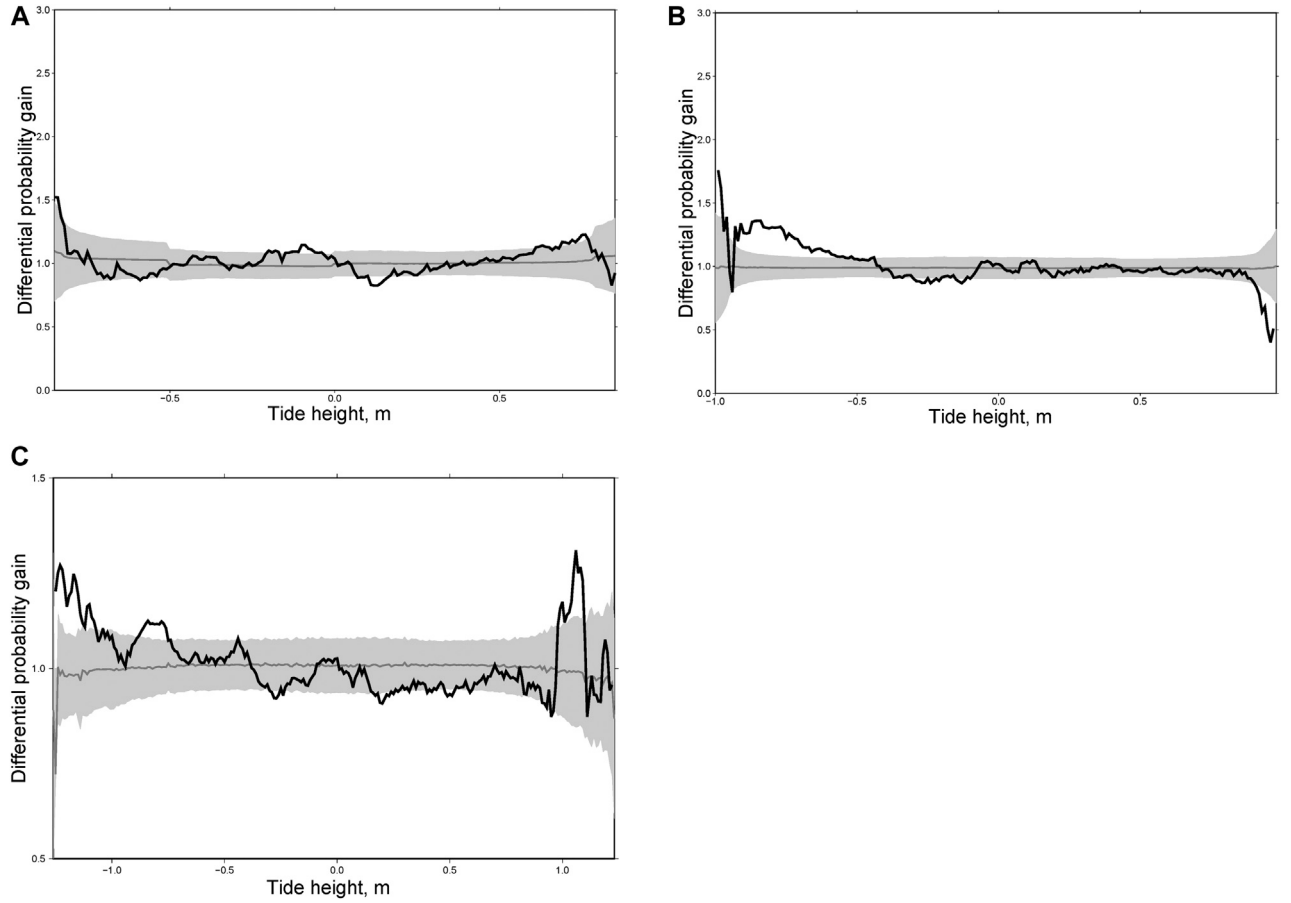

FIGURE 11 | Differential probability gain functions for two aftershock sequences in New Zealand following the earthquakes of M = 6.3, June 21, 1992 **(A)**; M = 7.8, November 13, 2016 **(B)**; and the integral differential probability gain function for six sequences with normal slip of main shocks **(C)**.

In order to check if our results could have been obtained by chance, we estimated the confidence interval of the DPG estimates. For each aftershock sequence we generated 10,000 random synthetic catalogues that satisfy the Omori-Utsu law with parameters determined from the real catalogue, and repeated the procedure for determining the DPG with each synthetic catalogue. Synthetic catalogues were constructed in a standard way for a non-stationary Poisson point process with successive times found using a random number generator:

$$t_{i+1} = t_i - \frac{\log(\xi)}{\lambda(t_i)}$$

where ξ is a random number uniformly distributed in (0,1), and intensity $\lambda(t)$ is given by the Omori-Utsu formula. We started at $t_0 = t_c/100$ and did not take into account events with $t_0 < t_c$, similarly to the analysis of the real catalogue. To each event we assigned the epicenter coordinates of the j-th event from the real aftershock sequence, randomly choosing an integer j uniformly distributed in (**1**, N), where N is the number of events in the real sequence. Finally, for each interval ($h–dh$, $h + dh$) of the tide height, we determined the mean and standard deviation of DPG from 10,000 values. If the value of the DPG falls outside the limits of the confidence interval determined in this way, the deviation of the DPG based on real data from 1.0 can be considered significant.

SEISMIC DATA

We investigated 16 aftershocks sequences of shallow earthquakes off Kamchatka, 1971–2013 (**Table 2**, **Figure 6A**). We used seismic data from the earthquake catalogue produced by the Kamchatka Branch of the Geophysical Survey of the Russian Academy of Sciences (Chebrov et al., 2016) for the period between 1962 and 2016 (http://www.emsd.ru/sdis/earthquake/catalogue/catalogue.php). Most of the main shocks are thrust events (**Figure 6A**; **Table 2**). For New Zealand we considered aftershock sequences of 15 large (M ≥ 6) earthquakes that had at least 100 aftershocks, near New Zealand, 1979–2016 (aftershocks hypocenter data of GeoNet, Earthquake Commission and GNS Science of New Zealand, available at: http://quakesearch.geonet.org.nz; **Table 3**, **Figure 6B**). **Tables 2**,**3** show the main parameters of these aftershock sequences.

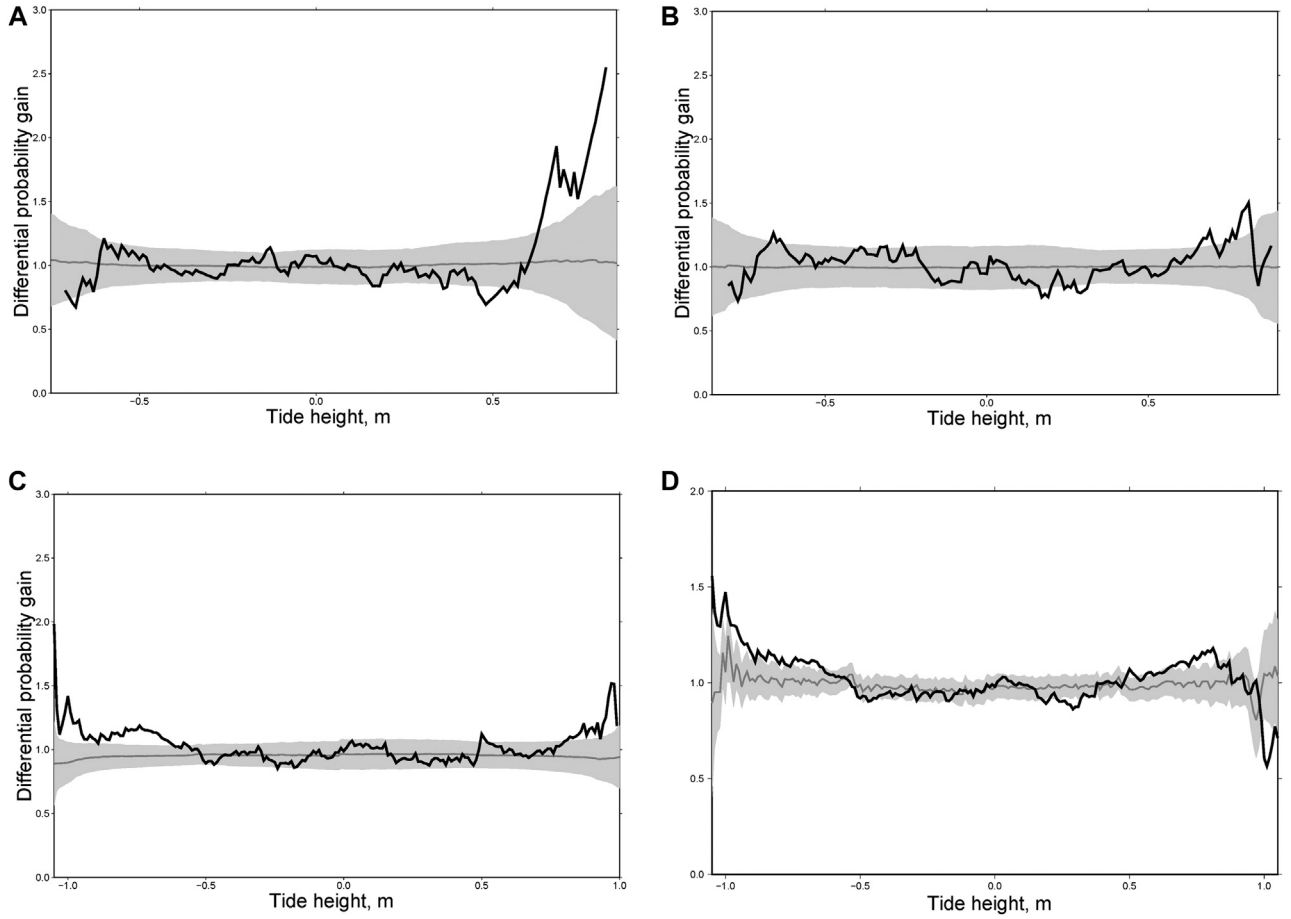

FIGURE 12 | The differential probability gain functions for three aftershock sequences in New Zealand following the strike-slip earthquakes of M = 6.4, May 25, 1981 **(A)**; M = 6.7, December 30, 1984 **(B)**; M = 6.5, July 21, 2013 **(C)**; and integral differential probability gain function for four sequences from strike-slip earthquakes **(D)**.

Figures 6A,B show a map of maximum ocean tide amplitude with resolution 0.125°. For Kamchatka near the coast, the amplitude of the ocean tides reaches 2 m, whereas for New Zealand it varies between 1.4 and 3 m, occasionally more. In Kamchatka all mainshock epicenters lie in the ocean, while for New Zealand some of the main shocks are on land, having a sufficient number of aftershocks in the ocean. Next, the quality of the catalogue for New Zealand is better, the magnitude of completeness M_c is generally smaller, and this generally results in a larger number of aftershocks to study and produces a better statistical significance of results compared with Kamchatka. The quality of hypocenter location in the catalogues is not important for our analysis. The spatial variation of the tide heights in all considered aftershock areas do not exceed 0.01 m in Kamchatka, and 0.02 m except earthquakes of 1993 and November 2016 in New Zealand; for those two earthquakes the spatial variation is about 0.07 m (**Figure 1**). The accuracy of the determinations of times of events (s) is very high when considered in relation to the time scale of tides (h).

RESULTS

Aftershock sequences have been identified for 16 (M ≥6) events with epicenters near Kamchatka (see **Figure 6A**; **Table 2**) and 15 (M ≥6) events with epicenters near New Zealand (see **Figure 6B**; **Table 3**) using the methods described above. For these sequences we estimated M_c and t_c as described in Section "Magnitude of completeness M_c and time of completeness t_c", and used these parameters to estimate c and p in 1 as described in Section "Modelling the aftershock rates" using data during the first month after the main shocks (**Tables 2**, **3**). Then for rectangular 0.2° × 0.2° boxes in the ocean we estimated the modeled aftershock rates λ_{ij} in (t_c, 720 h) within the aftershock areas and time intervals of 0.2 h assuming no impact of tides (**Eq. 1**), counted the actual aftershock numbers ω_{ij}, and used the FES 2004 program to find ocean tide heights h_{ij}. Finally, using **Eq. 2**, for all sequences we calculated the differential probability gain as a function of tide height. Everywhere we used the value dh = 0.15 m. We estimate also the confidence intervals

for DPG using random catalogues as described in *Differential Probability Gains*.

The Kamchatka Region

Figure 7 shows differential probability gain functions for four large earthquakes (M = 6.7, December 28, 1984; M = 6.3, July 10, 1987; M = 6.8, March 2, 1992; M = 6.8, February 28, 2013). Although the differential probability gain function shape may vary from one sequence to another, all examples demonstrate a clear increase of the function at high water (>0.5 m). A similar effect is observed for all sequences, with slightly less pronounced effect for the earthquakes of M = 7.8, December 15, 1971 and M = 7.8, December 5, 1997 (**Figure 8**). For those two earthquakes, the maximum of the DPG function is also observed at low water (near −1 m). We have constructed also the integral differential probability gain function for Kamchatka (**Figure 9**). **Eq. 2** was applied to all spatial boxes and time spans corresponding to several earthquakes. This analysis shows a clear maximum impact of the ocean tides at high water (>0.5 m).

New Zealand

Focal mechanisms of large earthquakes in New Zealand are different: mostly normal events in the north, thrusts in the south, and strike-slip earthquakes in the middle. Accordingly, we divided the main shocks into three groups: thrust faults (**Figure 10**), normal faults (**Figure 11**) and strike-slip faults (**Figure 12**). For each group we calculated individual and integral differential probability gain functions as we did for the Kamchatka sequences. As can be seen from **Figures 10**, for thrust faults the most general phenomenon consists in an increasing rate of aftershocks at high water (>0.5 m). A similar effect was found for Kamchatka (**Figures 7–9**) where almost all large earthquakes considered here were of the thrust type. For normal fault type earthquakes there is no effect at high water. In contrast, we observed a maximum of DPG at low water (<−0.5 m, **Figure 11**). A similar effect was observed for aftershocks following the earthquakes of M = 7.8, December 15, 1971 and M = 7.8, December 5, 1997 in Kamchatka (**Figure 8**). For strike-slip earthquakes the maximum of DPG functions is reached at high water for all sequences (>0.5 m). At low water, high DPG values were clearly observed for aftershocks of the M = 6.5 earthquake of July 21, 2013 (<−0.5 m, **Figure 12C**). These results demonstrate an impact of ocean tides on seismicity in the zones of large earthquakes within a period of 30 days after them. This highlights certain limitations to the analysis. The rupture zone of a large earthquake is in an excited state, so the impact of relatively weak disturbances, such as tides, may be stronger there than in the entire region.

LIMITATIONS OF THE ANALYSIS

In the analysis we used a model of ocean tides. The actual tide heights may be slightly different. However, continuous direct measurements do not exist at the moment. Another shortcoming of our analysis is that we could not ascertain the role of aftershock depth. This was mostly due to lack of data below the magnitude of completeness. An unreliable depth determination for offshore earthquakes is another factor. Accordingly, the physical model of the relationships found is very preliminary.

DISCUSSION AND CONCLUSION

In the present study we used the differential probability gain approach (Shebalin et al., 2012; Shebalin et al., 2014) to estimate quantitatively the change in aftershock rate at various levels of ocean tides, relative to an average Omori-Utsu model that supposes no dependence on tides. The differential probability gain function is a numeric factor indicating how much the rate of aftershocks is increased or decreased on average at specific values of the tide heights. The value one indicates no impact. We consider the impact of ocean tides only, because their effect is several times larger than the effect of solid Earth tides in the regions under consideration. Variations of vertical stresses of 10–20 kPa due to ocean tides for the coast of Kamchatka and New Zealand fall within the range of the effect of stresses on seismicity according to laboratory experiments (Lockner and Beeler, 1999). Similar variations due to Earth tides at shallow depths (<50 km) are only approximately 1 kPa, i.e., one order of magnitude less (Varga and Grafarend, 2017).

We considered aftershock sequences of large (M ≥6) earthquakes off Kamchatka, 1971–2013 (16 sequences) and New Zealand, 1979–2016 (15 sequences). For all sequences we disregarded data within a few first minutes or hours after main shocks, in which the catalogue usually remains incomplete even for relatively large magnitudes. Only aftershocks with epicenters in the ocean were used. In these regions, the amplitudes of ocean tides are large, and their influence is a few times or tens of times larger than the effects of Earth tides. The observed increase in the rate of aftershocks at high and/or low water demonstrated a significant effect of ocean tides on seismicity. One important feature that distinguishes this study from most others is that we studied the heights rather than the phases of ocean tides. Moreover, the goal of this study was to find quantitative estimates of the increase in seismicity rate at specific heights of the ocean tides. The effect varies from place to place and for different focal mechanisms. The main result consists in finding a significant change in seismicity rates at tide heights more than 0.5 m relative to the baseline, positive or negative. For normal fault earthquakes the effect is stronger at low water, for thrust events mostly at high water, and for strike-slip earthquakes at high and/or low water.

Although the differential probability gains function shape may vary from one sequence to another, we observed a clear tendency of increasing aftershock rate by about two times at either low or high water. As an explanation of this effect, we can suggest friction reduction on a fault due to vertical stress decreasing at low waters and due to increased pore pressure at high waters. For normal faults an increase in aftershock rate was observed at low water, and thus the friction reduction mechanism due to the unloading of vertical stress is more likely. For thrust earthquakes, an increase in aftershock rate was observed at high water, and in that case

increased pore pressure is the preferable mechanism. For strike-slip events with intermediate stresses both mechanisms can operate.

The main practical result of this study is a quantitative assessment of the effect of ocean tides on earthquake rate. Although the results were obtained for aftershocks, we may suppose that similar dependences are valid for all seismic events. Of course, this needs additional validation, but potentially opens a way to take into account ocean tides for time-dependent seismic hazard assessment.

DATA AVAILABILITY STATEMENT

The raw data supporting the conclusions of this article will be made available by the authors, without undue reservation.

AUTHOR CONTRIBUTIONS

PS provided the design and application of the differential probability gain tests. AB designed and performed calculations of the ocean tide heights.

FUNDING

We acknowledge the support from Russian Science Foundation Grant No. 20-17-00180.

ACKNOWLEDGMENTS

We acknowledge the New Zealand GeoNet project and its sponsors EQC, GNS Science and LINZ, and Kamchatka Branch of the Geophysical Survey of Russian Academy of Sciences for providing data used in this study. We are grateful to the authors of the FES 2004 for letting us use this software. We thank the reviewers for constructive comments which helped to improve the manuscript significantly.

SUPPLEMENTARY MATERIAL

The Supplementary Material for this article can be found online at: https://www.frontiersin.org/articles/10.3389/feart.2020.559624/full#supplementary-material.

REFERENCES

Arabelos, D. N., Contadakis, M. E., Vergos, G., and Spatalas, S. (2016). Variation of the Earth tide-seismicity compliance parameter during the recent seismic activity in Fthiotida, central Greece. *Ann. Geophys.* 59 (1), 102. doi:10.4401/ag-6795

Baranov, A. A., Baranov, S. V., and Shebalin, P. N. (2019). A quantitative estimate of the effects of sea tides on aftershock activity: Kamchatka. *J. Volcanol. Seismol.* 13 (1), 56–69. doi:10.1134/S0742046319010020

Beeler, N. M., and Lockner, D. A. (2003). Why earthquakes correlate weakly with the solid Earth tides: effects of periodic stress on the rate and probability of earthquake occurrence. *J. Geophys. Res. Solid Earth* 108 (B8), 2156–2202. doi:10.1029/2001JB001518

Burton, P. (1986). Geophysics: is there coherence between Earth tides and earthquakes? *Nature* 321 (6066), 115. doi:10.1038/321115a0

Cao, A. M., and Gao, S. S. (2002). Temporal variations of seismic b-values beneath northeastern Japan Island Arc. *Geophys. Res. Lett.* 29, 481–482. doi:10.1029/2001GL013775

Chebrov, V. N., Droznina, S. Ya., and Senyukov, S. L. (2016). *Kamchatka and the commander islands in Zemletryaseniya v Rossii v 2014 godu (Earthquakes in Russia in 2014)*. Obninsk, Russia: GS RAN, 60–66.

Chen, H.-J., Chen, C.-Y., Tseng, J.-H., and Wang, J.-H. (2012a). Effect of tidal triggering on seismicity in Taiwan revealed by the empirical mode decomposition method. *Nat. Hazards Earth Syst. Sci.* 12, 2193–2202. doi:10.5194/nhess-12-2193-2012

Chen, L., Chen, J. G., and Xu, Q. H. (2012b). Correlation between solid tides and worldwide earthquakes M C 7 since 1900. *Nat. Hazards Earth Syst. Sci.* 12, 587–590. doi:10.5194/nhess-12-587-2012

Cochran, E. S., Vidale, J. E., and Tanaka, S. (2004). Earth tides can trigger shallow thrust fault earthquakes. *Science* 306, 1164–1166. doi:10.1126/science.1103961

Crockett, R. G., Gillmore, M. G. K., Phillips, P. S., and Gilbertson, D. D. (2006). Tidal synchronicity of the December 26, 2004 Sumatran earthquake and its aftershocks. *Geophys. Res. Lett.* 33, L19302. doi:10.1029/2006GL027074

Datta, A., and Kamal, K. (2012). Triggering of aftershocks of the Japan 2011 earthquake by Earth tides. *Curr. Sci.* 102 (5), 792–796. doi:10.2307/24084467

Ekström, G., Nettles, M., and Dziewonski, A. M. (2012). The global CMT project 2004–2010: Centroid-moment tensors for 13,017 earthquakes. *Phys. Earth Planet. In.* 200–201, 1–9. doi:10.1016/j.pepi.2012.04.002

Emter, D. (1997). Tidal triggering of earthquakes and volcanic events. *Tidal Phenomena* 66, 293–309. doi:10.1007/BFb0011468

Hainzl, S. (2016). Rate-dependent incompleteness of earthquake catalogs. *Seismol Res. Lett.* 96 (2A), 337–344. doi:10.1785/0220150211

Hardebeck, J. L., Nazareth, J. J., and Hauksson, J. (1998). The static stress change triggering model: constraints from two southern California aftershock sequences. *J. Geophys. Res. Solid Earth* 103, 24427–24437. doi:10.1029/98JB00573

Heaton, T. H. (1975). Tidal triggering of earthquakes. *Geophys. J. Roy. Astron. Soc.* 43, 307–326. doi:10.1111/j.1365-246X.1975.tb00637.x

Heaton, T. H. (1982). Tidal triggering of earthquakes. *Bull. Seismol. Soc. Am.* 72, 2181–2200. doi:10.1111/j.1365-246X.1975.tb00637.x

Helmstetter, A., Kagan, Y. Y., and Jackson, D. (2006). Comparison of short-term and time-independent earthquake forecast models for southern California. *Bull. Seismol. Soc. Am.* 96 (1), 90–106. doi:10.1785/0120050067

Holschneider, M., Narteau, C., Shebalin, P., Peng, Z., and Schorlemmer, D. (2012). Bayesian analysis of the modified Omori law. *J. Geophys. Res.* 117, B05317. doi:10.1029/2011JB009054

Ide, S., and Tanaka, Y. (2014). Controls on plate motion by oscillating tidal stress: evidence from deep tremors in western Japan. *Geophys. Res. Lett.* 41, 3842–3850. doi:10.1002/2014GL060035

Ide, S., Yabe, S., and Tanaka, Y. (2016). Earthquake potential revealed by tidal influence on earthquake size–frequency statistics. *Nat. Geosci.* 9, 834–837. doi:10.1038/ngeo2796

Klein, F. W. (1976a). Earthquake swarms and the semidiurnal solid earth tide. *Geophys. J. Int.* 45, 245–295. doi:10.1111/j.1365-246X.1976.tb00326.x

Klein, F. W. (1976b). Tidal triggering of reservoir-associated earthquakes. *Eng. Geol.* 10, 197–210. doi:10.1016/0013-7952(76)90020-x

Knopoff, L. (1964). Earth tides as a triggering mechanism of earthquakes. *Bull. Seismol. Soc. Am.* 54, 1865–1870.

Le Provost, C., Lyard, F., Molines, J. M., Genco, M. L., and Rabilloud, F. (1998). A hydrodynamic ocean tide model improved by assimilating a satellite altimeter-derived data set. *J. Geophys. Res.* 103, 5513–5529. doi:10.1029/97JC01733

Le Provost, C., Genco, M. L., Lyard, F., Vincent, P., and Canceil, P. (1994). Spectroscopy of the world ocean tides from a finite element hydrodynamic model. *J. Geophys. Res.* 99, 777–797. doi:10.1029/94JC01381

Le Provost, C., and Vincent, P. (1986). Some tests of precision for a finite element model of ocean tides. *J. Comput. Phys.* 65, 273–291. doi:10.1016/0021-9991(86)90209-3

Lin, C. H., Yeh, Y. H., Chen, Y. I., Liu, J. Y., and Chen, K. J. (2003). Earthquake clustering relative to lunar phases in Taiwan. *Terr. Atmos. Ocean Sci.* 14, 289–298. doi:10.3319/TAO.2003.14.3.289(T)

Lockner, D. A., and Beeler, N. M. (1999). Premonitory slip and tidal triggering of earthquakes. *J. Geophys. Res.* 104 (B9), 20133–20151. doi:10.1029/1999JB900205

Lyard, F., Lefèvre, F., Letellier, T., and Francis, O. (2006). Modelling the global ocean tides: a modern insight from FES 2004. *Ocean Dynam.* 56, 394–415. doi:10.1007/s10236-006-0086-x

Malin, S. R. C., and Chapman, S. (1970). The determination of lunar daily geophysical variations by the Chapman-Miller method. *Geophys. J. Roy. Astron. Soc.* 19, 15–35. doi:10.1111/j.1365-246X.1970.tb06738.x

Metivier, L., de Viron, O., Conrad, C. P., Renault, S., Diament, M., and Patau, G. (2009). Evidence of earthquake triggering by the solid earth tides. *Earth Planet Sci. Lett.* 278, 370–375. doi:10.1016/j.epsl.2008.12.024

Molchan, G. M., and Dmitrieva, O. E. (1992). Aftershock identification: methods and new approaches. *Geophys. J. Int.* 109, 501–516. doi:10.1111/j.1365-246X.1992.tb00113.x

Molchan, G. M. (1991). Structure of optimal strategies in earthquake prediction. *Tectonophysics* 193, 267–276. doi:10.1016/0040-1951(91)90336-Q

Morgan, W. J., Stoner, J. O., and Dicke, R. H. (1961). Periodicity of earthquakes and the invariance of the gravitational constant. *J. Geophys. Res.* 66 (11), 3831–3843. doi:10.1029/JZ066i011p03831

Nikolaev, V. A. (1996). Relationships between seismicity and the phases of multiple and difference tidal waves. *Dokl. Akad. Nauk.* 349 (3), 389–394.

Nikolaev, V. A. (1994). The response of large earthquakes to the phases of earth tides. *Izvestiya Phys. Solid Earth* 11, 49–55.

Rydelek, P. A., Sacks, I. S., and Scarpa, R. (1992). On tidal triggering of earthquakes at Campi Flegrei. *Italy. Geophys. J. Int.* 109, 125–137. doi:10.1111/j.1365-246X.1992.tb00083.x

Saltykov, V. A., Ivanov, V. V., and Kugaenko, Y. A. (2004). The action of earth tides on seismicity prior to the Mw 7.0 November 13, 1993, Kamchatka earthquake. *Izvestiya Phys. Solid Earth* 7, 25–34.

Saltykov, V. A. (2014). Tidal effects and amplitude-dependent dissipation in seismicity. *Fizicheskaya Mezomekhanika* 17, 103–110.

Scholz, C. H., Tan, Y. J., and Albino, F. (2019). The mechanism of tidal triggering of earthquakes at mid-ocean ridges. *Nat. Commun.* 10, 2526. doi:10.1038/s41467-019-10605-2

Schuster, A. (1897). On lunar and solar periodicities of earthquakes. *Proc. Roy. Soc. Lond.* 61, 455. doi:10.1098/rspl.1897.0060

Shebalin, P., and Baranov, S. (2017). Long-delayed aftershocks in New Zealand and the 2016 M 7.8 Kaikoura earthquake. *Pure Appl. Geophys.* 174 (10), 3751–3764. doi:10.1007/s00024-017-1608-9

Shebalin, P. N., Narteau, C., and Baranov, S. V. (2020). Earthquake productivity law. *Geophys. J. Int.* 222 (2), 1264–1269. doi:10.1093/gji/ggaa252

Shebalin, P. N., Narteau, C., and Holschneider, M. (2012). From alarm-based to rate-based earthquake forecast models. *Bull. Seismol. Soc. Am.* 102, 64–72. doi:10.1785/0120110126

Shebalin, P. N., Narteau, C., Zechar, J. D., and Holschneider, M. (2014). Combining earthquake forecasts using differential probability gains. *Earth Planets Space* 66, 37. doi:10.1186/1880-5981-66-37

Shudde, R. H., and Barr, D. R. (1977). An analysis of earthquake frequency data. *Bull. Seismol. Soc. Am.* 67, 1379–1386.

Simpson, J. F. (1967). Earth tides as a triggering mechanism for earthquakes. *Earth Planet Sci. Lett.* 2, 473–478. doi:10.1016/0012-821X(67)90192-6

Souriau, M., Souriau, A., and Gagnepain, J. (1982). Modeling and detecting interactions between Earth tides and earthquakes with application to an aftershock sequence in the Pyrenees. *Bull. Seismol. Soc. Am.* 72, 165–180.

Stein, R. S. (1999). The role of stress transfer in earthquake occurrence. *Nature* 402, 605–609. doi:10.1038/45144

Stein, R. S. (2004). Tidal triggering caught in the act. *Science* 305 (5688), 1248–1249. doi:10.1126/sciencee.1100726

Stroup, D. F., Bohnenstiehl, D. R., Tolstoy, M., Waldhauser, F., and Weekly, R. T. (2007). Pulse of the seafloor: tidal triggering of microearthquakes at 9°50′N East Pacific Rise. *Geophys. Res. Lett.* 34, L15301. doi:10.1029/2007GL030088

Tanaka, S., Ohtake, M., and Sato, H. (2002). Evidence for tidal triggering of earthquakes as revealed from statistical analysis of global data. *J. Geophys. Res.* 107 (B10), 2211. doi:10.1029/2001JB001577

Tanaka, S., Ohtake, M., and Sato, H. (2004). Tidal triggering of earthquakes in Japan related to the regional tectonic stress. *Earth Planets Space* 56, 511–515. doi:10.1186/BF03352510

Tanaka, S. (2010). Tidal triggering of earthquakes precursory to the recent sumatra megathrust earthquakes of December 26, 2004 (Mw 9.0), March 28, 2005 (Mw 8.6), and September 12, 2007 (Mw 8.5). *Geophys. Res. Lett.* 37, L02301. doi:10.1029/2009GL041581

Tanaka, S. (2012). Tidal triggering of earthquakes prior to the 2011 Tohoku-Oki earthquake (Mw 9.1). *Geophys. Res. Lett.* 39, L00G26. doi:10.1029/2012GL051179

Tolstoy, M., Vernon, F. L., Orcutt, J. A., and Wyatt, F. K. (2002). Breathing of the seafloor: tidal correlations of seismicity at Axial volcano. *Geology* 30, 503–506. doi:10.1130/0091-7613(2002)030<0503:BOTSTC>2.0.CO;2

Tsuruoka, H., Ohtake, M., and Sato, H. (1995). Statistical test of the tidal triggering of earthquakes: contribution of the ocean tide loading effect. *Geophys. J. Int.* 122, 183–194. doi:10.1111/j.1365-246X.1995.tb03546.x

Utsu, T. A. (1961). Statistical study on the occurrence of aftershocks. *Geophys. Mag.* 30, 521–605.

Varga, P., and Grafarend, E. (2017). Influence of tidal forces on the triggering of seismic events. *Pure Appl. Geophys.* 175, 1–9. doi:10.1007/s00024-017-1563-5

Varini, E., Peresan, A., and Zhuang, J. (2020). Topological comparison between the stochastic and the nearest-neighbor earthquake declustering methods through network analysis. *J. Geophys. Res. Solid Earth* 125, e2020JB019718. doi:10.1029/2020JB019718

Vergos, G. S., Arabelos, D., and Contadakis, M. E. (2015). Evidence for tidal triggering on the earthquakes of the Hellenic Arc, Greece. *Phys. Chem. Earth* 85–86, 210–215. doi:10.1016/j.pce.2015.02.004

Vidale, J. E., Agnew, D. C., Johnston, M. J. S., and Oppenheimer, D. H. (1998). Absence of earthquake correlation with Earth tides: an indication of high preseismic fault stress rate. *J. Geophys. Res.* 103 (B10), 24567–24572. doi:10.1029/98JB00594

Wiemer, S., and Wyss, M. (2000). Minimum magnitude of completeness in earthquake catalogs: examples from Alaska, the western United States, and Japan. *Bull. Seismol. Soc. Am.* 90, 859–869. doi:10.1785/0119990114

Wilcock, W. S. (2001). Tidal triggering of microearthquakes on the Juan de Fuca ridge. *Geophys. Res. Lett.* 28, 3999–4002. doi:10.1029/2001GL013370

Woessner, J., and Wiemer, S. (2005). Assessing the quality of earthquake catalogues: estimating the magnitude of completeness and its uncertainty. *Bull. Seismol. Soc. Am.* 95, 684–698. doi:10.1785/0120040007

Yurkov, E. F., and Gitis, V. G. (2005). On relationships between seismicity and the phases of tidal waves. *Izvestiya Phys. Solid Earth* 4, 4–15.

Zaliapin, I., and Ben-Zion, Y. (2013). Earthquake clusters in southern California I: identification and stability. *J. Geophys. Res.* 118 (6), 2847–2864. doi:10.1002/jgrb.50179

Conflict of Interest: The authors declare that the research was conducted in the absence of any commercial or financial relationships that could be construed as a potential conflict of interest.